Optimizing Jet Energy Resolution with Jets Simulated from Test-Beam Data

John P. Borders

Restrictions introduced in the optimization of the energy response of the DØ calorimeter to hadrons worsen hadron energy resolution by a total of about 6% for the sampling term S over that found using an unrestricted optimization.[1] The worst degradation occurs when the weights for the electromagnetic layers are fixed to values that provide the best resolution for single electrons. Another restriction that produces a clear loss in resolution is when the weights are required to be independent of the energy of the incident particle. These restrictions can produce similar or perhaps even more detrimental effects on jet resolution. Finally, the somewhat intuitive prediction that the Default Set of weights would be best for jet resolution leads to a loss in single hadron resolution of about 9-11% in the sampling term S. Without a detailed knowledge of the composition of jets, it is difficult to predict the impact of such restrictions. Unfortunately, jets of precise energy cannot be produced in test beams, and consequently cannot be studied in a calorimeter.

However, production of jets can be modeled using Monte Carlo generation based on QCD theory. The individual hadronic fragments of such jets can be taken from a library of data obtained in the test beam, summed to form a jet, and then propagated through the detector to simulate the response of the DØ calorimeter to jets. In this analysis, we use such simulations to study the effects that the restrictions placed on single-hadron optimization produce on jet resolution. In particular, we study the effects on jet response using the default weights from previous analysis,[1] and investigate possible alternate schemes for improving jet resolution.

1 Generating Test Beam Jets

The Particle Library, based on data from the test beam, was formed to provide the individual particles needed for generating jets.[2] The Particle Library contains both electron and hadron data over the full range of energies studied at the test beam, but only at the position corresponding to η=0.05 and ϕ=3.16 in the DØ calorimeter. Extrapolations, also described in Appendix B, are performed to shift the scales and locations of particles to the appropriate energies and positions of specified jet constituents. These particles are then superimposed to form complete jet events which mimic DØ events on a cell-by-cell level.

To specify the structure of the jets to be built by the Particle Library, partons were generated at minimum transverse energies of 20, 30, 40, 50, 63, 80, 100, 120, 150, 175, and 200 GeV, using the Isajet program. After fragmentation and radiation, the jet with the highest p_T from the collision was selected and stored in a file specifying the energy, type, and the η

and ϕ for each constituent. For each specified minimum energy, this process produced a group of jets distributed around the minimum energy. The specified set of minimum energies had been selected so that, taken all together, the Isajet events had a broad range of energies with essentially uniform distribution between about 15 and 225 GeV. We will refer to these seed events as "Isajet events", to distinguish them from the test-beam jet events ("TB jets"), which are constructed using the Isajet events.

For each Isajet event, the Particle Library was used create TB jets that are similar to jets seen in the DØ detector. Because the library is limited to particles at η=0.05, only central jets could be simulated accurately (see Appendix B for a discussion of the differences between the assembled jets and DØ jets). For each specified Isajet event, 200 TB jets were constructed from data randomly selected from the Particle Library).[2]

2 Parameters of Jet Response

Because a non-linearity in the energy response of calorimeters to jets can, in principle, be easily corrected, we will concentrate on issues relevant to the resolution of the DØ calorimeters in optimizing TB jets. The jet resolution was fitted to the same generic equation that was used for parametrizing the energy resolution of single particles.[1] However, because the noise term in the jet cannot be simply the sum over the noise of individual hadrons, the N parameter must be handled differently for TB jets.

For the resolution of hadrons in single-particle test beam data, the noise term N was equated to the expected standard deviation of an appropriate pedestal distribution, and thereby the number of degrees of freedom in the fit was reduced.[1] When the contributions from individual particles are added together to form TB jets, the magnitude of the noise in a typical TB jet will usually be far greater than for a single particle, and will increase with the multiplicity of the jet. Since the multiplicity of a jet also depends upon jet energy, the noise in TB jets will have a dependence upon incident jet energy. This is an artificial feature of building jets from individual particles, and does not reflect the true noise of the calorimeter.

Noise in TB jets was estimated by merging data for inspill pedestal events on a cell-by-cell basis, using the same correction algorithms that were applied to the cells occupied by

the particles in a TB jet, using the following procedure. First, an inspill-pedestal library was created in parallel with the Particle Library: this contained inspill pedestal events from the test beam. For each initial Isajet event that had been used to create TB jets, we then created a jet-pedestal event by adding events from the pedestal library for all individual particles in the Isajet event. Essentially, a TB jet was built, but with cells containing only pedestal signals, rather than ionization energy. This procedure overestimates the noise seen in a DØ jet-pedestal event by an amount equivalent to that in a TB jet relative to a real (DØ) jet, providing a dependence of the standard deviation of a jet-pedestal event on incident jet energy. The mean value of the jet-pedestal events is, of course, still zero. A plot of the N parameter (i.e., the average width of the jet-pedestals) vs. incident jet energy, in 5 GeV intervals, is shown in Fig. 1. A fit to the energy dependence is also shown in the figure, and is given by:

$$N(E) = P_1 + P_2 \ln(E) \tag{1}$$

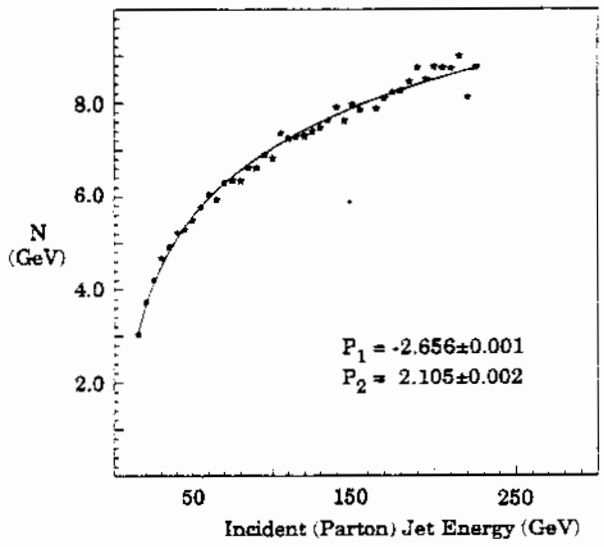

Figure 1 Standard deviation of "artificial" inspill pedestals (jet-pedestal events) as a function of incident jet energy

Due to the way the data in the Particle Library are scaled for low incident energies (see Appendix B), the noise for a single particle (≈1.9 GeV) does not have to correspond exactly to the noise at smallest jet energy in Fig. 1. Also, the same scaling techniques cause the

above fit to become non-physical at energies less than about 10 GeV (for example, N(5 GeV) ≈ 0). Since the particle library is only used down to 15 GeV, this will not present a problem.

Using Eq. 1 in the standard expression for resolution,[1] we obtain a modified form that we can use to extract the other parameters of the fractional resolution:

$$\left(\frac{\sigma(E)}{\mu(E)}\right)^2 = C^2 + \frac{S^2}{E} + \frac{\left[P_1 + P_2 \ln(E)\right]^2}{E^2} \qquad (2)$$

Single hadron analysis indicated that the default weights should be used for building jets. Here we will examine the jet properties found using these weights.[1] Figure 2(a) gives a plot of the reconstructed jet energy vs. the incident jet energy, including a linear fit through the data, and the parameters for the fit (the statistical errors on these are very small). In Fig. 2(b) we show the result of the linear fit compared to the fractional energy difference.

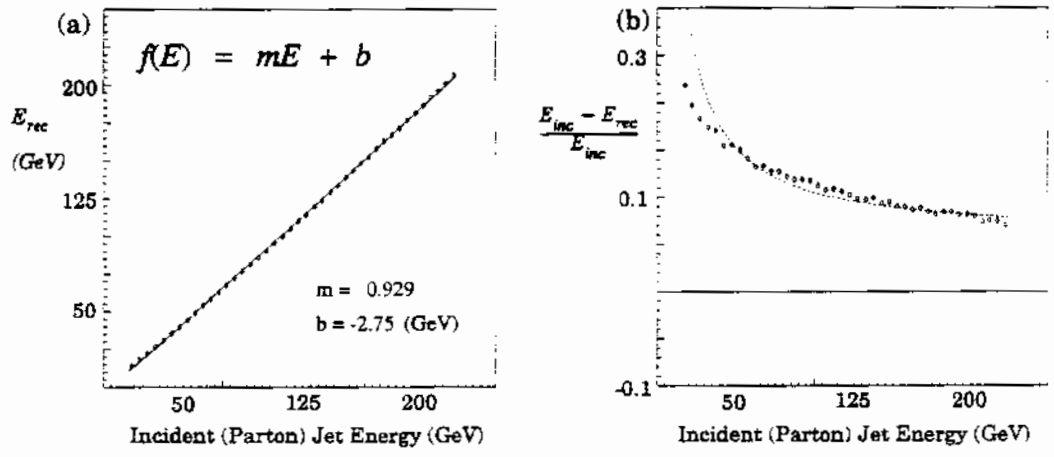

Figure 2 Reconstructed energies obtained using default weights at η=0.45

As seen in Fig. 2, the response of the calorimeter to energy is not completely linear, and has both a large offset and a slope that differs significantly from 1.0. In order to correct for these effects, a simple second-order polynomial can be fitted to the response, and the reconstructed energy can be corrected using the resulting function. In this chapter we correct all energies in this manner. The corrected energy for the default weights, in terms of the plot

of fractional energy differences, is given in Fig. 3(a), and the relative resolution is shown in Fig. 3(b).

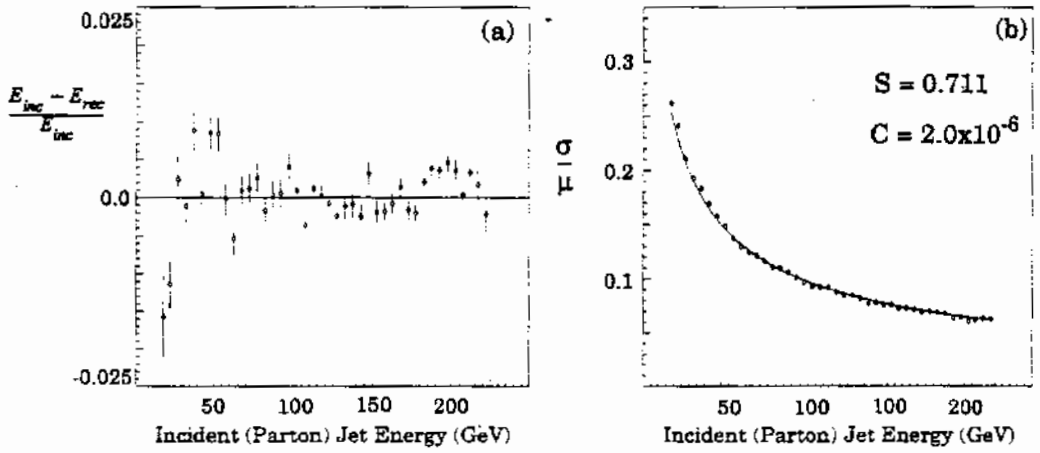

Figure 3 (a) Relative differences and (b) relative resolution for corrected reconstructed jet energies

The fit that corresponds to the corrected data in Fig. 3 is:

$$E_{rec}^{corr} = P_1 + P_2 E_{rec} + P_3 E_{rec}^2 \qquad (3)$$

with P_1 = 2.42 GeV, P_2 = 1.13, and P_3 = -3x10^{-4} GeV^{-1}, and where E_{rec} is the uncorrected reconstructed energy shown in Fig 2.

Figure 3 shows that the data at the lower end of the energy range have more scatter than at the central region. This is due to the fact that the simulation of DØ jets becomes less accurate at the lowest energies. This breakdown of the simulation is mainly due to the scaling of the lowest energy particles, and an arbitrary cutoff of low-energy jet constituents used when building the TB jets.[2]

The Isajet jets in this analysis were required to be in the central region of the calorimeter at the Isajet generation stage. However, due to the way the particle library produces the coordinates of TB jets by shifting the particles at η=0.05 to the appropriate coordinates, TB jets will not vary in structure, regardless of pseudo-rapidity of the Isajet jet.

3 Optimization of Jet Resolution

All results in the following optimizations will be presented in terms of sampling factors, relative to the default weights. (The default weights correspond to dE/dx weights for the hadronic layers, and EM-layer weights chosen to optimize the response to electron).

Five different optimization schemes (OS) were implemented to try to improve the energy resolution of TB jets. OS-1 simply varies the relative scales between the EM and hadronic layers, and otherwise uses the default weights. OS-2 allows all weights to vary, and provides a single constant offset δ for the simultaneous optimization of all jet energies. OS-3 admits weights that depend on the reconstructed jet energy, and OS-4 allows weights that depend on the fraction of total reconstructed jet energy deposited in the electromagnetic layers (EM fraction). Finally, OS-5 implements a sequential optimization of energy-dependent and EM fraction-dependent variations. A summary of the various optimization schems is included in Table 1, and the details of the separate optimizations are given below.

Table 1 Summary of optimization schemes (OS)

OS	Parameters allowed to vary	# parameters	constant offset δ
1	scale factors describing relative contributions of EM and hadronic sections	2	set to zero
2	energy-independent weights describing the relative contributions of all layers	8	varies
3	parameters describing the energy-dependence of 8 layer weights	16	set to zero
4	parameters describing the EM fraction-dependence of 8 layers weights and a constant offset δ	18	varies
5	parameters describing the EM fraction-dependence and energy-dependence of 8 layer weights and a constant offset δ	8	varies for EM dependence set to zero for energy-dependence

3.1 Optimization of Relative Electromagnetic and Hadronic Scales (Scheme

OS-1)

Just as in the case of single hadrons, the relative scales of the signals from the electromagnetic and hadronic sections were varied, keeping the default weights for the individual layers in the two sections. The reconstructed jet energy (E^k_{rec}) is found from:

$$E^k_{rec} = \alpha_{em} E^k_{em} + \alpha_{had} E^k_{had} \qquad (4)$$

where E^k_{rec} is the reconstructed energy for TB jet event k, E^k_{em} and E^k_{had} are the sums of the energies found in the electromagnetic and hadronic layers, respectively (calculated using the default weights), and α_{em} and α_{had} are parameters that are varied using our standard optimization routine for all TB jet events (all energies). The resultant values of α_{em} and α_{had} are given in Table 2. Uncertainties on these values are not included: since the scales are found through the optimization procedure used to find sampling weights, the uncertainties are of little use in evaluating the results, due to the correlations between them.

Table 2 Optimized relative scales (OS-1)

α_{em}	1.25
α_{had}	0.98

3.2 Full Optimization Without Energy Dependence (Scheme OS-2)

The TB jet resolution was optimized simultaneously over the full range of energies, resulting in the set of 8 sampling factors and the constant offset δ, given in Table 3. This scheme assumes that the weights are independent of jet energy.

Table 3 Fully optimized, energy-independent sampling factors (OS-2)

Calorimeter Layer	Sampling Factors
EM1	2.443
EM2	1.163
EM3	0.856
EM4	1.335
FH1	1.006
FH2	0.895
FH3	0.839
CH	0.758
δ (GeV)	3.325

3.3 Sampling Factors as a Function of Reconstructed Jet Energy (Scheme OS-3)

The energy-dependent weights were found as follows:

1. The default reconstructed energy (E_{def}) was calculated using the default weights in Eq. 5.9.
2. The events were divided into 5 GeV bands of E_{def}.
3. A set of sampling factors were obtained for each band E_{def}.
4. The sampling factors were fitted to a linear function of E_{def}.

A constant offset δ is not allowed in this optimization, since such an offset is not suitable for optimizations over small energy ranges. The calculated sampling weights, along with the linear fits to E_{def}, are shown as a function of reconstructed energy in Fig. 4. All eight fits are superimposed in Fig. 4(i) to demonstrate the correlations between the weights as a function of energy, along with a line at unity. The parameters for these functions, along with the statistical uncertainties on them, are given in Table 4.

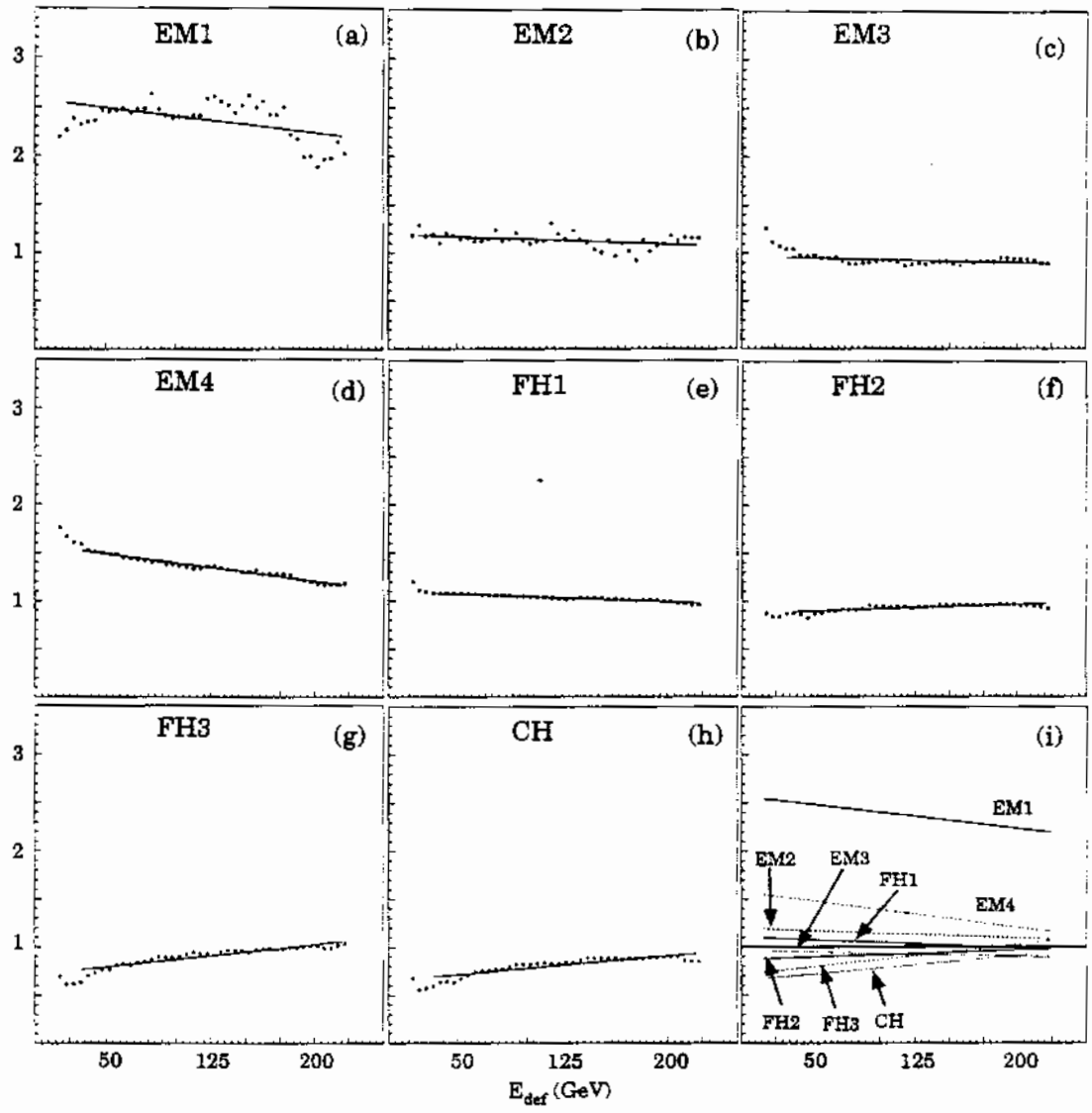

Figure 4 Sampling factors as a function of reconstructed energy (OS-3). The fits are to linear functions of the form $P_1 + P_2 E_{def}$ (see Table 4).

As can be seen in Fig. 4, the sampling factors at the extreme ranges of the energy scales do not seem to follow the trend observed in the center regions. By changing the ranges for the fits, we have determined that restricting the fits to the trend established by the central energy regions results in the best overall resolutions. The functions in the figures are plotted only over the energy ranges used in the fits.

It can also be seen from Fig. 4 that some of the sampling factors do not seem to depend linearly on energy. We have tried to fit the sampling factors with a more complex energy dependence, but found that using a linear fit provides similar overall resolution, and produces a more linear energy response. We have consequently chosen the simplest parameterization for this study.

Table 4 Parameters describing energy-dependence of sampling factors (OS-3)

	P_1	P_2 $(x10^{-3})$ (GeV^{-1})
EM1	2.571±0.003	-1.69±0.02
EM2	1.195±0.003	-0.51±0.02
EM3	0.963±0.004	-0.33±0.03
EM4	1.579±0.004	-1.88±0.03
FH1	1.104±0.004	-0.56±0.03
FH2	0.870±0.004	0.49±0.03
FH3	0.714±0.004	1.56±0.03
CH	0.652±0.004	1.28±0.03

It is interesting that all weights appear to approach unity at highest energies, as shown in Fig. 4(i). This would suggest that these weights should provide the greatest improvement in reconstructed energy resolution at lowest energies.

3.4 Sampling Factors that Depend on Jet EM Fraction (OS-4)

The weights that depend on EM fraction were found as follows. Starting out with the default E_{def} values, as discussed in Section 3.3, we defined F_{EM} as the fraction of the energy in a TB jet that was reconstructed in the EM section. The F_{EM} values for all events were divided in bands of 0.04 width, to obtain a set of sampling factors (and a constant offset δ) for all events (independent of energy) within each band of EM fraction. These factors were then fitted as a function of F_{EM}.

The sampling factors as a function of EM fraction in a TB jet are shown in Fig. 5, along with the linear functions used in the fit. The parameters for these functions, along with their statistical errors, are given in Table 5.

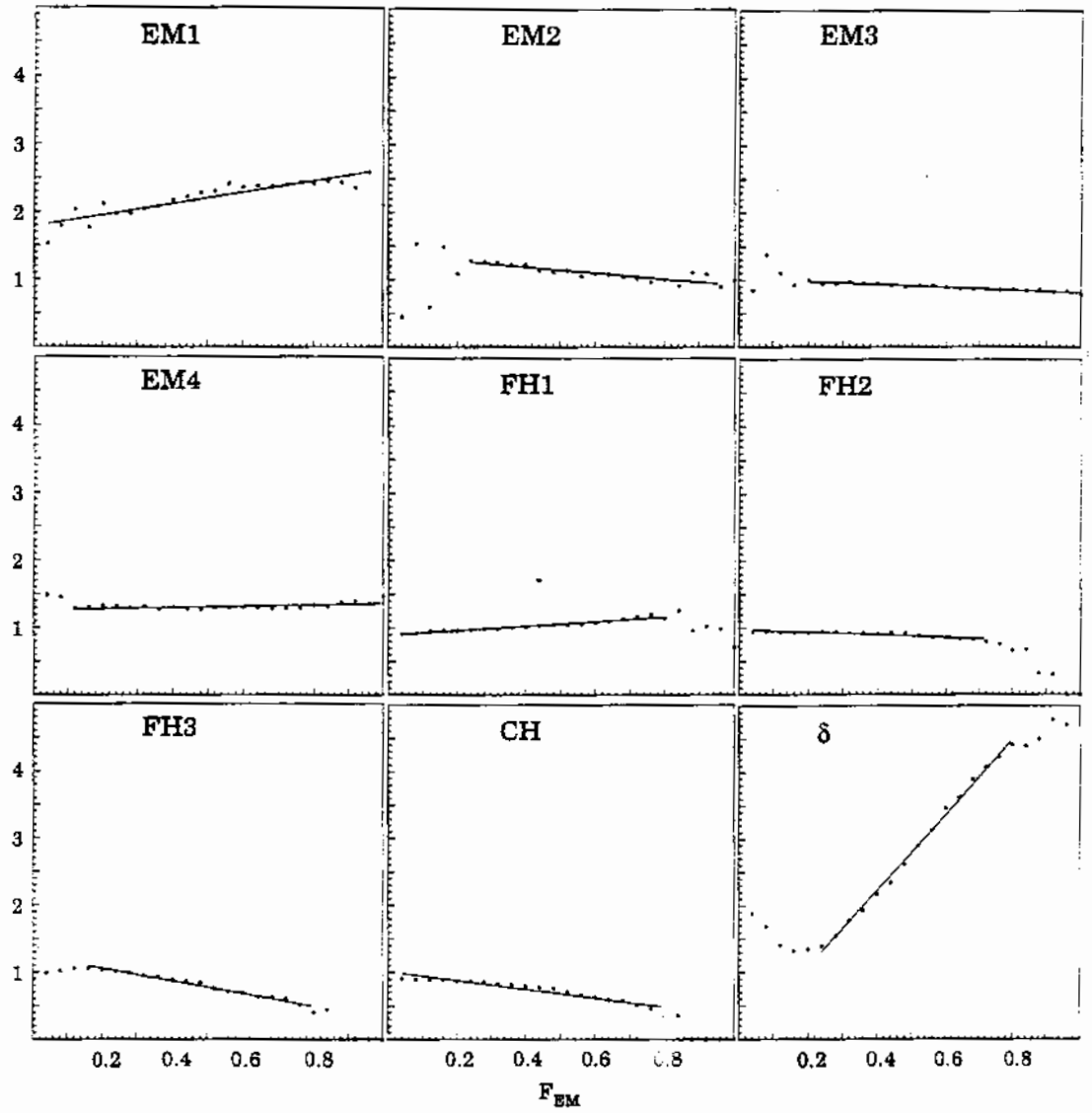

Figure 5 Sampling factors as a function of the fraction of the reconstructed energy in a TB jet that is deposited in the EM section. The fits are to linear functions of the form $P_1 + P_2 F_{EM}$ (see Table 5)

As seen in Fig. 5, the sampling factors for $F_{EM} \leq 0.2$ and $F_{EM} \geq 0.8$, (especially for δ) show marked deviations from the trend established in the rest of the range. This is caused primarily by the characteristic patterns of energy deposition for jets in these regions. For example, a jet with more than 90% of its energy in the electromagnetic section, will have little energy in CH that could be used to sharpen the CH sampling factor. Also, it should be

recognized that jets usually deposit ≈ 0.5 of their energy in the EM section, so the low incidence of jets with > 0.9 of the total energy in either section makes the optimizations in these regions statistically inadequate (the statistical uncertainties on these points are connected to the correlations between weights, so these uncertainties are not shown in the plots).

Table 5 Energy-independent sampling factors (OS-4) obtained from linear fits to the EM energy fraction in TB jets (with statistical uncertainties from the fits)

	P_1	P_2 ($\times 10^{-1}$ GeV^{-1})
EM1	1.788±0.004	8.37±0.07
EM2	1.370±0.007	-4.47±0.1
EM3	1.016±0.006	-2.11±0.09
EM4	1.263±0.005	0.96±0.08
FH1	0.896±0.005	3.34±0.09
FH2	0.977±0.005	-1.99±0.1
FH3	1.247±0.006	-9.40±0.1
CH	1.011±0.005	-6.60±0.1
δ	-0.057±0.001	56.9±0.1

3.5 Sampling Factors that Depend on both EM Fraction and Reconstructed Energy (Scheme OS-5)

In order to exploit information about both the energy of the TB jet and its EM fraction, optimizations were carried out that included both dependences. First, the factors found in Sec. 3.4 (for OS-4) were applied to data, and then sampling factors were recalculated as a function of reconstructed energy as was done in Sec. 3.3. However, the reconstructed energy for this optimization was taken as the corrected energy E_{EM} found using the parameters discussed in Sec. 3.4, rather than E_{def}.

Plots of the final factors as a function of E_{EM} are shown Fig. 6, and the parameters for fits to a linear dependence on E_{EM} are shown in Table 6. We see in Fig. 6 that after correcting for the EM fraction, the sampling factors are all close to unity over our entire energy range, indicating that applying both energy-dependent and EM fraction-dependent corrections is not significantly more useful than using only one of these corrections.

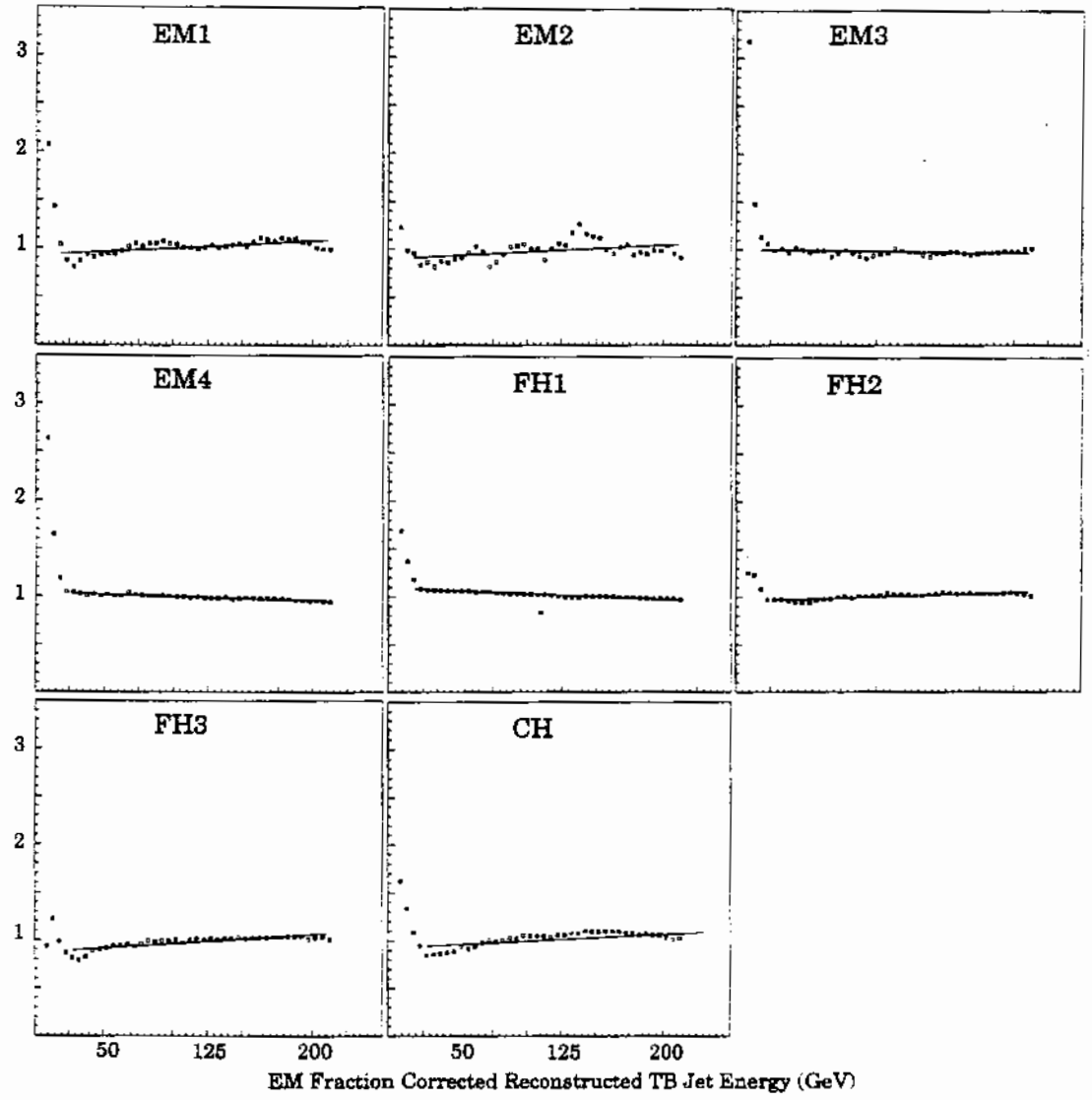

Figure 6 Sampling factors as a function of EM-fraction corrected reconstructed energy (OS-5). The fits are to linear functions of the form $P_1 + P_2 E_{rec}$ (see Table 6).

We also see in Fig. 6 that the sampling weights for the lowest energies show a marked difference from those for the higher energies. This indicates that using both EM fraction and energy-dependent corrections should have a negative impact on lowest-energy jets.

Table 6 Energy dependent sampling factors obtained from linear fits to the energy after EM-fraction corrections (OS-5) (with statistical uncertainties from the fits)

	P_1	P_2 ($\times 10^{-4}$ GeV^{-1})
EM1	0.927±0.003	7.65±0.02
EM2	0.898±0.003	7.29±0.02
EM3	0.998±0.003	-1.75±0.02
EM4	1.042±0.004	-4.17±0.03
FH1	1.094±0.003	-6.07±0.02
FH2	0.957±0.004	4.57±0.03
FH3	0.869±0.004	9.71±0.03
CH	0.927±0.004	6.90±0.03

3.6 Corrections to Reconstructed Energies

As stated in Sec. 2, all reconstructed TB jet energies for the default as well as for the optimized parameters were corrected using a second-order polynomial in E_{rec} (Eq. 3). The plots of the nominal parton energies vs. reconstructed energies are given in Fig. 7, and the parameters for the fits indicated are given in Table 7.

Table 7 Parameters from fits of second-order polynomial in reconstructed TB jet energy to the incident parton energy (with statistical errors from the fits)

OS-#	P_1 (GeV)	P_2	P_3 ($\times 10^{-4}$ GeV^{-1})
Default	2.41±0.02	1.13±0.01	-3.12±0.03
1	2.22±0.02	1.02±0.01	-2.16±0.02
2	-1.96±0.02	1.04±0.01	-0.96±0.02
3	1.37±0.02	0.97±0.01	1.70±0.02
4	-2.07±0.02	1.05±0.01	1.53±0.02
5	-1.97±0.02	1.04±0.01	-1.03±0.02

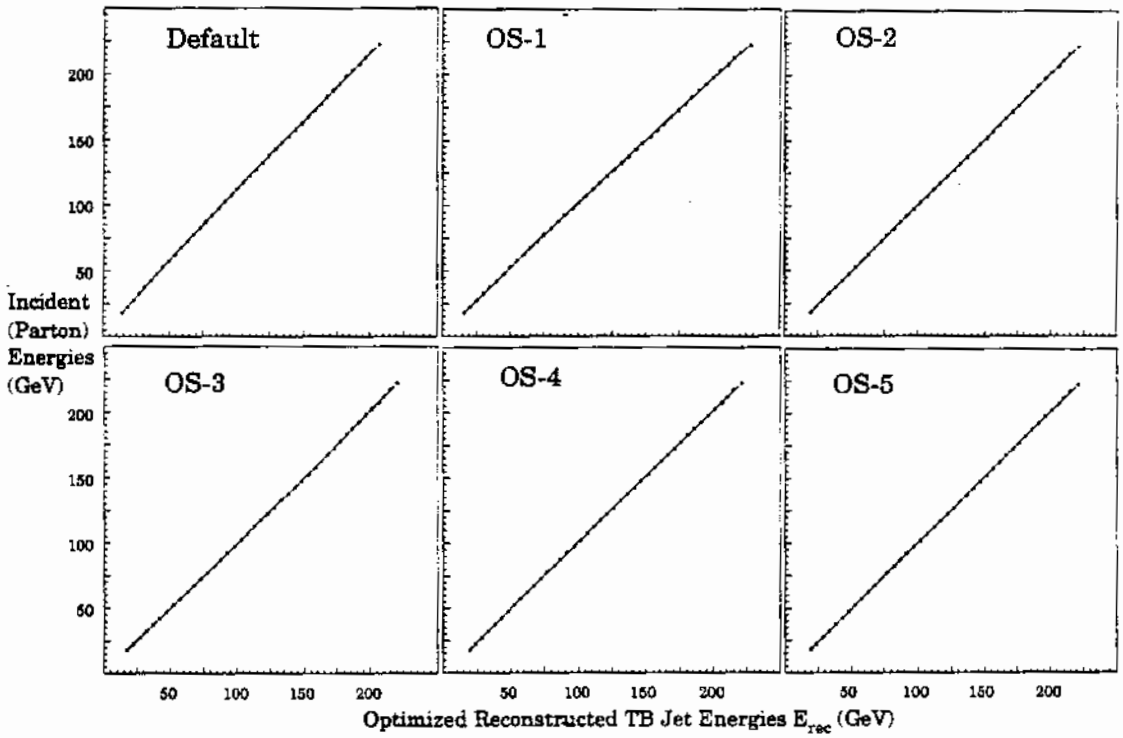

Figure 7 Nominal parton energy as a function of reconstructed TB jet energy for various optimizations. The fits are to second-order polynomial functions of E_{rec}.

These plots give little indication of the differences between the different response distributions. The parameters in Table 7 give greater detail about the differences between the various optimizations.

4 Judging the Success of the Optimization Schemes on Resolution

To investigate the effect of the optimization schemes on reconstructed TB jet energy resolution, a separate set of data, consisting of 218,500 events, was generated from the Particle Library. The corrections obtained from the optimization schemes were then applied as follows:

1. For each event, we calculated the default reconstructed TB jet energy E_{def} using the default weights.
2. Choosing some optimization scheme, the appropriate sampling factors were determined for any given E_{def}

3. These factors were then applied to the layer energies to find the optimized reconstructed energies E^i_{opt}, for any given optimization scheme i.
4. Finally, the corrections to the reconstructed TB jet energy, based on Table 7, were applied to determine the final energies E^i_{corr}.

These corrected and optimized energies were then compared with the parton energies to determine the jet resolution as a function of incident energy, as explained here. The reconstructed energies E^i_{corr} were separated into bands of 5 GeV. In parallel with the rescaling of energies of singles hadrons that was based on the measurements using PWCs, we also rescaled all the values of E^i_{corr} to the mean parton energy in the band. This eliminated any smearing in E^i_{corr} due to the spread in parton energies. We then calculated the standard deviation σ(E) and mean μ(E) for each band of E^i_{corr} energies. The parameters of the resolution were then extracted by fitting Eq. (2) to the values of σ/μ. The parameters S and C from the fits, and their statistical uncertainties, are given in Table 8, and the corrected data for the various schemes with the fitted functions are shown in Fig. 8.

Table 8 Parameters describing resolution of reconstructed and corrected TB jet energies

OS-#	S (%/√E)	C (%)
Default	71.15±0.004	0.002±0.003
1	58.18±0.01	1.98±0.002
2	48.19±0.01	2.32±0.002
3	43.42±0.01	2.76±0.001
4	37.03±0.01	3.32±0.002
5	35.18±0.01	3.40±0.001

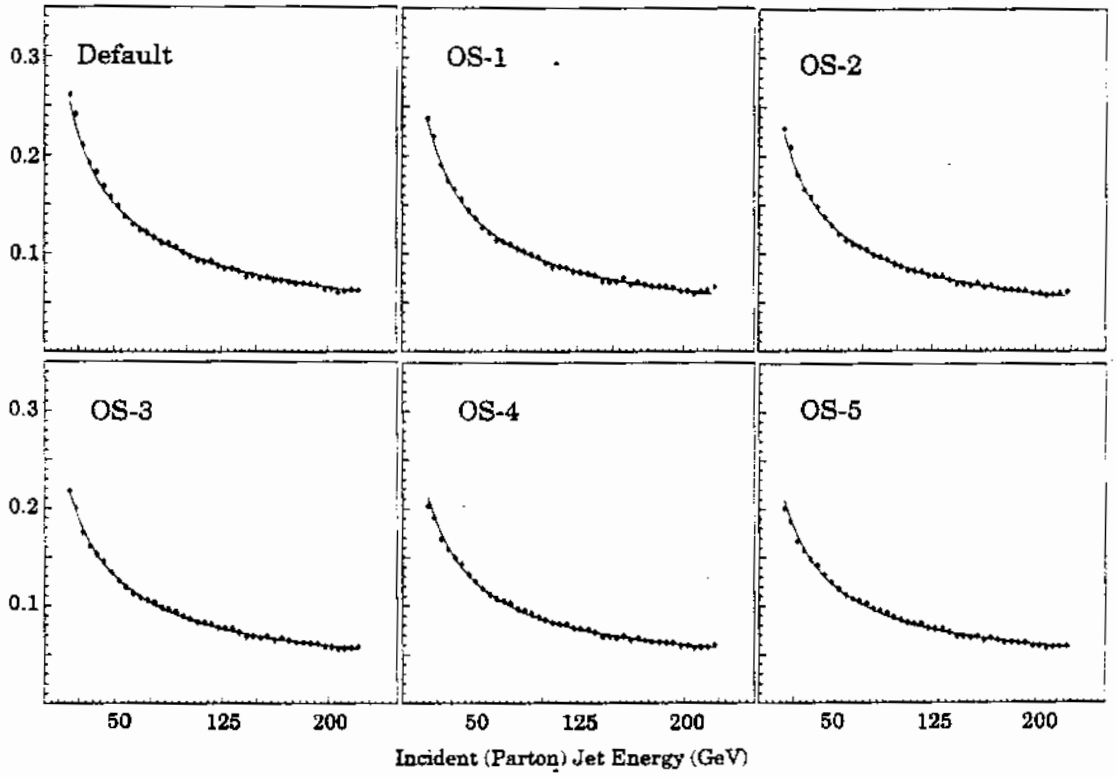

Figure 8 Fractional resolutions for TB jets as a function of incident energy for the various optimization schemes. Fits of the data are to Eq. 2

To show a simple example of the improvement in resolution given by the optimization, we include a plot of the distribution of a single jet energy peak (E=150 GeV) for both the default weights and the OS-5 weights in Fig. 9.

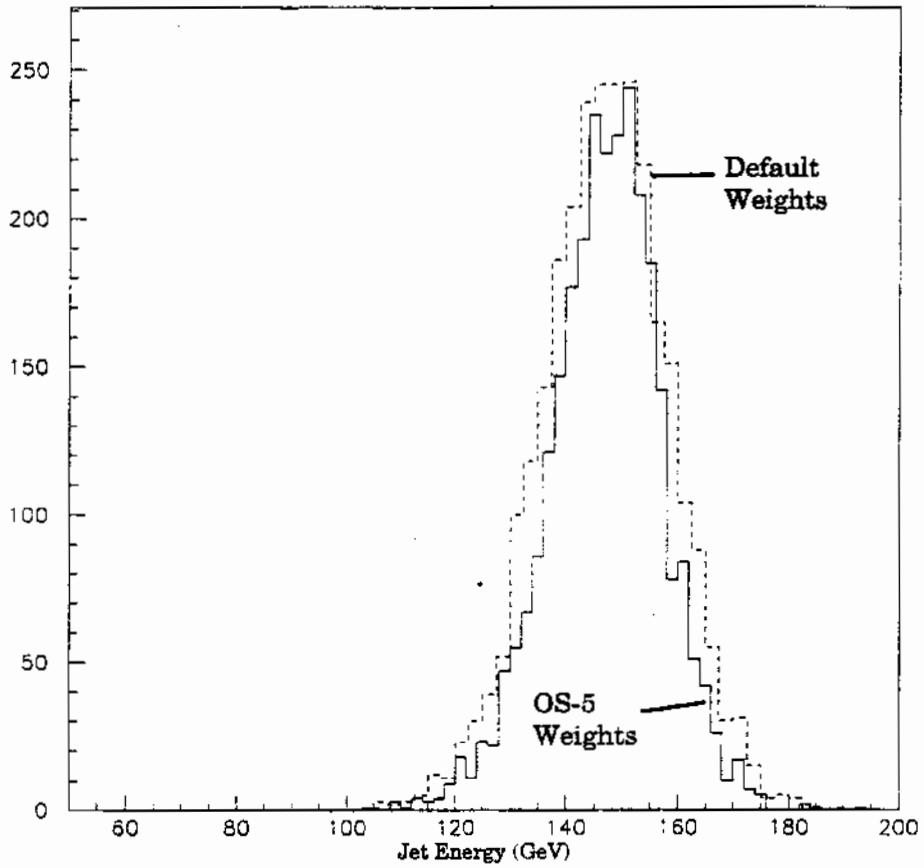

Figure 9 150 GeV Jet Response Distribution for Default Weights and OS-5 Weights

Because of the similarity of the plots in Fig. 8, and the fact that an increase in C can be compensated by a decrease in S in Table 8, if is difficult to gauge any improvement in jet energy resolution from the different optimization schemes. We therefore provide in Fig. 10 a comparison of the resolutions for the various schemes relative to the case using the default parameters.

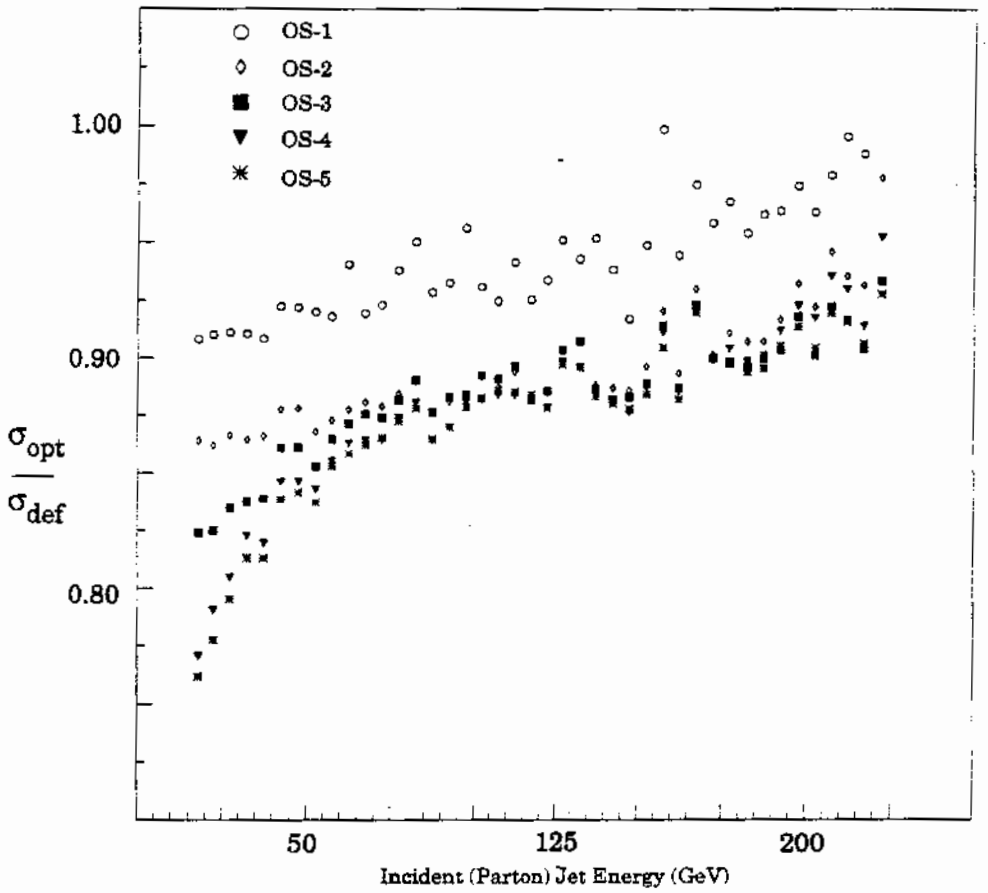

Figure 10 Ratio of optimized TB jet resolutions to the default values as a function of jet parton energy.

From Fig. 10, we see that while OS-1 improves the resolution over the default scheme, it is not as marked an improvement as those using the other schemes. The improvements for OS-2 to OS-5 are only slight at the highest energies, but more apparent at the lower energies. The OS-4 and OS-5 schemes appear to provide the best overall resolution.

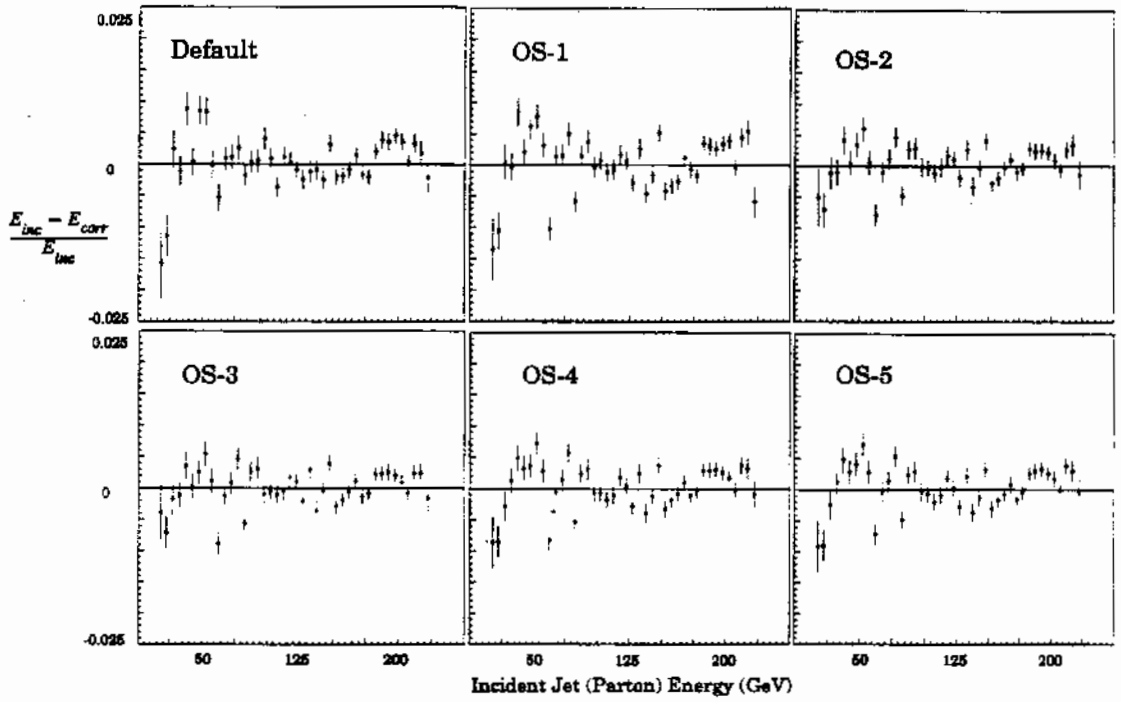

Figure 11 Fractional differences between the corrected reconstructed TB jet energies and incident parton energies, for different optimization schemes.

Fractional energy differences for the various optimization schemes are shown in Fig. 11. As can be seen in the figure, the fractional differences are all very similar, as expected, since all energy responses were corrected using a second-order polynomial in E_{rec}, (see Sec. 3.6). Nevertheless, these plots verify that the corrections are reasonable. (As we mentioned previously, when the sampling factors in Sections 3.3, 3.4, and 3.5 were fitted to third or fourth-order polynomials in E_{rec}, these fractional differences were not as well-behaved.)

From the results of this analysis, we see that the energies of TB jets more closely reflect the original parton characteristics (as shown by jet energy resolution) when we implement our optimization schemes. Thus, the weights suggested by single-particle optimization can be improved upon by applying a more detailed knowledge of jet structure to test beam data.

References:

1. J. Borders, *Using Single Hadron Data to Optimize the Response of DØ Central Calorimeters for the Measurement of Hadronic Jet Energies*, DØ Note #1502 (1994).

2. J. Borders, *Structure of the DØ Particle Library and How it is Used to Simulate Jets*, DØ Note #2078 (1994).